

# Desirable Airfoil Characteristics for Large Variable-Speed Horizontal Axis Wind Turbines

P. Giguère

Graduate Research Assistant.

M. S. Selig

Assistant Professor.

Department of Aeronautical and  
Astronautical Engineering,  
University of Illinois at Urbana-Champaign,  
306 Talbot Laboratory,  
104 S. Wright Street,  
Urbana, IL 61801-2935

*In an effort to define the desirable airfoil characteristics for large variable-speed wind turbines, a systematic study was performed using a series of airfoils designed to have similar aerodynamic properties, except for the amount of lift, which varied over a wide range. For several airfoil combinations, blade shapes were designed for a 750-kW wind turbine with a 48.8-m diameter rotor using the optimization code PROPGA together with PROPID, which is an inverse design method for horizontal-axis wind turbines. Roughness effects, including the consideration of dirty-blade performance in the blade-shape optimization process, were also considered and are discussed. The results and conclusions reveal practical design implications that should aid in the aerodynamic blade design of not only large but also other sizes of variable-speed wind turbines.*

## 1 Introduction

In the last decade, the development of airfoils for wind turbine applications has been given considerable attention. For instance, ongoing work at the National Renewable Energy Laboratory (NREL) has led to a series of over 25 specially tailored airfoils for horizontal-axis wind turbines (HAWTs) (Tangler and Somers, 1995). For the most part, the NREL effort and others, such as the work of Björk (1988), Hill and Garrad (1989), Madsen and Rasmussen (1992), and Timmer and Rooy (1992), have concentrated on the development of airfoils for stall-regulated wind turbines. The development of new airfoils for variable-speed, pitch-regulated machines, however, has received only little attention in the literature. Björk (1989) has performed one of the few studies on airfoil design for variable-speed HAWTs. More recently, Jamieson and Rawlinson-Smith (1994) considered high-lift airfoils for applications to all types of wind turbines (fixed speed, variable-speed, pitch or stall regulated). Consequently, although the unique airfoil design requirements for stall-regulated HAWTs are rather well established, desirable airfoil characteristics for variable-speed HAWTs have yet to be as clearly defined.

As a step toward identifying the desirable airfoil characteristics for variable-speed HAWTs, this paper presents a systematic study that involved the design of ten airfoils and their subsequent application to a three-blade variable-speed wind turbine having a diameter of 48.8 m (160 ft) and rated power of 750 kW. Section 2 describes the development of the airfoil series and corresponding performance characteristics. The blade shape optimization process is outlined in Section 3. Application of the overall approach is given in Section 4, and results from the optimized blade shapes are discussed. The desirable airfoil characteristics for large variable-speed HAWTs are explicitly outlined in Section 5.

It should be emphasized that the objective of this work was not to develop a series of airfoils or blade shapes for application. Instead, this work was undertaken to illustrate the application of the methodology and from the results define desirable airfoil characteristics for variable-speed HAWTs. It is expected that the conclusions presented here can be also applied to medium size and perhaps even small variable-speed HAWTs; however,

a similar airfoil/blade-shape optimization procedure as outlined will need to be performed.

## 2 Airfoil Series: Design and Analysis

It is well known that the outboard region of the blade provides a large fraction of the energy production. Thus, in this study, particular focus was placed on the outboard portion of the blade. A series of five primary airfoils and five tip airfoils were designed as depicted in Fig. 1. The primary and tip airfoils were, respectively, 14 percent and 11 percent thick and used at the 75 percent and 100 percent blade stations, hence the notation 75 and 100 in the airfoil name. Both series were designed to cover a range of maximum lift coefficients  $C_{l,max}$  resulting in a range of maximum lift-to-drag ratios  $C_l/C_d$  for constant Reynolds numbers  $Re$ . The suffix in the name indicates the approximate  $C_l$  corresponding to the best  $C_l/C_d$ , e.g., "12" indicates  $C_l \approx 1.2$  for best  $C_l/C_d$ . For the inboard region of the blade, the 24 percent thick S818 (Tangler and Somers, 1995) was used for the first 30 percent of the blade span.

The primary and tip airfoil series were systematically designed using PROFOIL (Selig and Maughmer, 1992), which is an inverse airfoil design method that allows the user to prescribe the desired velocity distribution from which the corresponding airfoil shape is determined. Each airfoil has a similar velocity distribution that differs mainly in the amount of aft loading. Consequently, the higher lift airfoils have greater pitching moment coefficients. For example, the 75-08 and 75-16 airfoils have zero-lift pitching moment coefficients of  $-0.07$  and  $-0.17$ , respectively. The design Reynolds number for the primary and tip airfoils was  $Re = 2.5 \times 10^6$ . The transition ramp was also systematically tailored to maintain low laminar separation bubble drag. Thus, the airfoils were not generated simply by geometric perturbations of the thickness and camber distributions. Since an inverse (aerodynamic) method was used, the aerodynamic characteristics of the airfoils are related, and in this sense the airfoils can be considered as a series from a performance perspective as will later be shown.

As described by Somers (1992) and Selig et al. (1995), in order to have limited sensitivity to leading-edge roughness, the airfoil must be designed to have natural transition take place close to the leading edge when the airfoil operates near  $C_{l,max}$ . This way, artificial transition caused by roughness owing to insect debris, rain, erosion, etc., will have limited effect on  $C_{l,max}$ . Such an airfoil design requirement, however, is of primary importance for stall-regulated wind turbines and

Contributed by the Solar Energy Division of THE AMERICAN SOCIETY OF MECHANICAL ENGINEERS for publication in the ASME JOURNAL OF SOLAR ENERGY ENGINEERING. Manuscript received by the ASME Solar Energy Division, Dec. 1996; final revision, Mar. 1997. Associate Technical Editor: P. S. Veers.

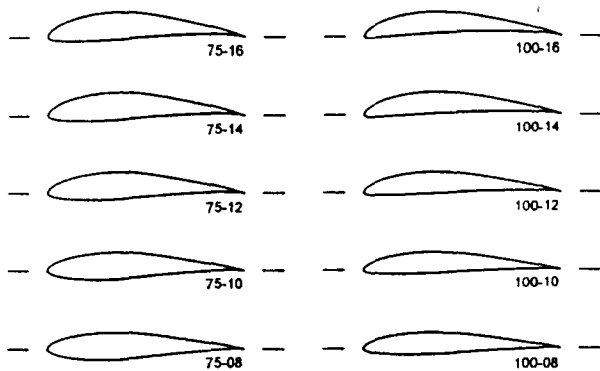


Fig. 1 Primary ( $r/R = 75$  percent and  $t/c = 14$  percent) and tip ( $r/R = 100$  percent and  $t/c = 11$  percent) airfoil series

does not limit roughness effects below stall. The sensitivity of variable-speed HAWTs to roughness depends mainly on the amount of laminar flow present on the upper surface of the airfoils used. An airfoil with a large amount of laminar flow will provide greater  $C_l/C_d$  performance when clean but will also suffer the most from roughness effects. Consequently, there is a trade-off between high maximum  $C_l/C_d$  performance when clean and larger penalty under dirty-blade conditions or more modest performance under clean conditions with a lesser penalty due to roughness effects. All of the airfoils designed for this study have natural transition take place near 30 percent chord at low lift coefficients. With leading-edge roughness, however, artificial transition near the leading edge results in a thicker boundary layer downstream. The added displacement thickness and momentum thickness (due to both the growth in the roughness region and subsequent longer run of turbulent flow) can effectively decamber the airfoil and cause trailing-edge separation, which will lower the lift coefficient as compared with the clean case. The selection of 30 percent is a compromise between clean and dirty-blade performance, which favors clean-blade conditions since it has been established that variable-speed wind turbines are less sensitive to roughness effects (Tangler and Somers, 1995; Tangler, 1996). Variable-speed wind turbines operate over a relatively limited  $C_l$  range and below stall, which make them much less susceptible to roughness effects as compared with stall and pitch-regulated machines.

XFOIL (Drela, 1989, 1990) was used to predict the airfoil performance characteristics. This computer code uses a panel method coupled with an integral boundary layer method that allows for the analysis of airfoils with free or fixed transition, laminar separation bubbles, and limited trailing-edge separation. All airfoils were analyzed under clean (free transition) conditions while only the 08, 12, and 16 airfoil series were analyzed under dirty-blade conditions. Drag polars are shown in Fig. 2 for the five primary and five tip airfoils at  $Re = 4 \times 10^6$ . The method used to simulate leading-edge roughness was to fix transition at two percent and five percent chord on the upper and lower surfaces, respectively. A similar approach, which also represents a worst case scenario, was also used by Björk (1989). For the clean condition over the Reynolds number range considered in this work, results predicted by XFOIL show good agreement with experiment below the onset of stall (Drela, 1989). Good agreement below stall is sufficient, because again variable-speed wind turbines operate below stall during normal operations. For rough blade conditions (fixed transition at the leading edge), however, some discrepancies between predictions and experiment do exist. In particular, the predicted loss in lift due to roughness is smaller than experiment. Thus, to model the

overall effects due to roughness on  $C_l$ , an empirical expression to properly account for the loss in lift given by

$$\Delta C_l = \begin{cases} -0.67(t/c) + 0.038 & \text{for series 08} \\ -0.80(t/c) + 0.029 & \text{for series 12} \\ -0.93(t/c) + 0.021 & \text{for series 16} \end{cases} \quad (1)$$

was used to correct the predicted lift coefficient. This correction is modeled in part after experimental data taken on the S805, S809, and S814 wind turbine airfoils tested at Delft (Somers, 1986, 1987, 1994).

Finally, in the blade-shape optimization process, the airfoil lift was interpolated linearly with angle of attack and Reynolds number, and the airfoil drag was interpolated linearly with angle of attack and logarithmically with Reynolds number. For spanwise stations positioned between two adjacent airfoil locations, linear interpolation on the distance was used to determine the final  $C_l$  and  $C_d$  values. Thus, since no approximations such as the use of a parabolic drag polar were used, the airfoil performance characteristics were modeled quite accurately.

### 3 Blade Shape: Design and Analysis

The blade-shape design process was performed in two stages as illustrated in the flow chart shown in Fig. 3. In the first stage, PROPGA (Selig and Coverstone-Carroll, 1996) was used to optimize the blade pitch as well as the blade chord and twist distribution for a selected airfoil combination, e.g., S818 (0 percent–30 percent station), airfoil 75-08 (75 percent) and airfoil 100-08 (100 percent). The gross annual energy production was used as the figure of merit to determine the optimum design. As shown in the flow chart, the lift coefficient and axial induction factor distributions for the optimized blades were then determined using PROPID (Selig and Tangler, 1995) in the analysis mode.

Briefly, PROPGA for wind turbine blade shape optimization is based on a robust parameter search technique—a genetic algorithm—that models Darwin's principle of the survival of the fittest. In the current implementation, 100 generations were considered, each of which were composed of 100 wind turbines. From one generation to the next, the better traits of particular wind turbines were passed on through "breeding." This process, once repeated over several generations, resulted in a design that maximized the gross annual energy production. More details of the method can be found in Selig and Coverstone-Carroll (1996).

The optimization process using PROPGA often led to blade shapes with an exceedingly high solidity inboard. For instance, the local solidity ( $\sigma = Bc/2\pi r$ ) at the 25 percent station was in some cases as high as 0.095 when values near 0.05 or less are more typical. Thus, a practical constraint was imposed by prescribing (in the second stage) an inboard lift coefficient distribution that was higher than the optimized case, thereby reducing the inboard solidity to values near 0.05. For all optimized cases, the axial induction factor distribution varied about a value of  $\frac{1}{3}$ —a value consistent with classic theory (Wilson, 1994). Thus, the axial induction factor distribution was prescribed to be a constant  $\frac{1}{3}$  for all cases.

The second stage in the design process involved using an inverse wind turbine design method, PROPID, to achieve the desired lift coefficient and axial induction factor distributions determined by PROPGA with the practical constraint on the lift coefficient inboard as described. The outboard lift coefficient distribution was based on PROPGA results. Some limited smoothing, however, was required since, as will later be discussed, the optimum blade was not particularly sensitive to the local lift coefficient.

The performance prediction method in PROPID and PROPGA is the widely used PROP code (Hibbs and Radkey,

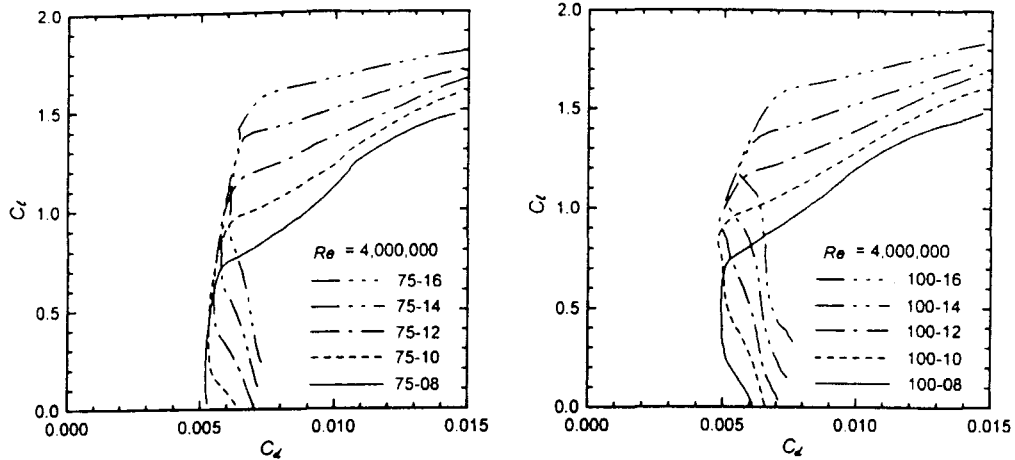


Fig. 2 Predicted drag polars for the five primary and five tip airfoils at  $Re = 4 \times 10^6$

1983) based on blade element/momentum theory. After two decades of use, it has become a wind industry standard. The gross annual energy prediction is based on the standard approach outlined by Wilson (1994) using a Rayleigh wind speed distribution.

#### 4 Results and Discussion

To examine the effects of using the various airfoils illustrated in Fig. 1, a case matrix was constructed as shown in Table 1. The first and last two digits correspond to the primary and tip airfoils, respectively. The cases in the lower left diagonal, for instance 16-08, were not considered because the optimized blades resulted in an undesirable flared tip, that is, a tip chord that was broader than the chord at the 75 percent station.

For all cases, a three-blade variable-speed wind turbine having a diameter of 48.8 m (160 ft) and rated power of 750 kW was considered. This size is comparable to many existing wind turbines. The results shown are for a tip-speed ratio TSR of 7, which is typical of wind turbines in this class. In determining the gross annual energy production, an average wind speed of 7.15 m/s (16 mph) and a cut-out velocity of 17.8 m/s (40 mph) were used.

**Blade Designs for Clean Conditions.** Figure 4 shows the blade chord and twist distributions, and Fig. 5 shows the  $C_l$  distributions for cases 08-08, 08-16, and 16-16 optimized for clean-blade conditions (using airfoil data for the free transition case). As might be expected, case 08-08 has a broad chord and a correspondingly low  $C_l$  distribution; whereas, case 16-16 has a narrow chord distribution and a relatively high  $C_l$  distribution. Case 08-16 is a mixture of the latter two, being similar to case 08-08 inboard and case 08-16 outboard.

Table 2 shows the gross annual energy production in percent relative to the case 08-08 (the baseline), having a gross annual

annual energy of 2473 MWh. As seen, although the airfoil family (root, primary and tip combination) significantly affects the blade solidity (see Fig. 4 and Table 3), the differences in the annual energy production are small, between 0 percent–1 percent, with case 16-16 showing the greatest gain. Although the gain is small, it is significant relative to that possible. Specifically, when the airfoil profile drag is set to zero, the annual energy for all cases is 2,556 MWh, which represents a gain of 3.4 percent and 2.4 percent relative to case 08-08 (baseline) and case 16-16, respectively. The power coefficients of the blade shapes presented in Fig. 4 over a broad range of TSR are shown in Fig. 6. As expected, the maximum power coefficients occur at the design TSR of 7 for the three rotors, and the maximum power coefficient ( $C_p$  of 0.534) is obtained with rotor 16-16. Furthermore, Fig. 6 indicates that small fluctuations in TSR from the design TSR does not significantly change the power coefficients. The rotor 08-08 provides the best off-design performance, which appears to be mainly related to the lift range of the primary airfoil.

Since case 16-16 corresponds to the blade with the highest  $C_l$  airfoils (Fig. 1) with the highest  $C_l/C_d$  (for constant  $Re$ ), it is not surprising to find that this case has the best performance. In general as either the primary or tip airfoil  $C_l/C_d$  or both increases, the performance improves as indicated in Table 2. It is interesting, however, to find that the operating  $C_l$  along the blade is below that for the best  $C_l/C_d$ . It can be seen by comparing Fig. 2 with Fig. 5 that the optimum  $C_l$  distributions (outboard) are below those corresponding to the best  $C_l/C_d$ . For reference, the airfoils in the outboard region of the blade for cases 08-08, 08-16, and 16-16 for a wind speed of 7.15 m/s (16 mph), operate at Reynolds numbers near  $3.5 \times 10^6$ ,  $2.7 \times 10^6$  and  $1.9 \times 10^6$ , respectively.

The result of having an optimum  $C_l$  distribution lower than that for best  $C_l/C_d$  for the corresponding  $Re$  can be understood

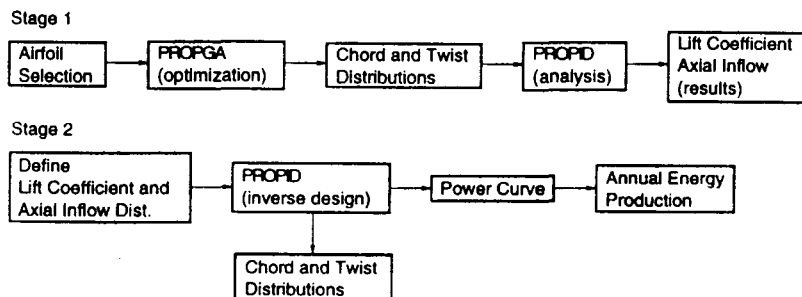


Fig. 3 Flow chart outlining the present design procedure

**Table 1 Case matrix showing the naming scheme corresponding to the primary and tip airfoil combinations considered**

		Tip Airfoil (100%)					
		100-08	100-10	100-12	100-14	100-16	
Primary Airfoil (75%)	75-08	08-08	08-10	08-12	08-14	08-16	
	75-10		10-10	10-12	10-14	10-16	
	75-12			12-12	12-14	12-16	
	75-14				14-14	14-16	
	75-16					16-16	

by first considering two equations from blade-element/momentum theory given by

$$\frac{a}{1-a} = \sigma C_l \frac{\cos \phi}{4 \sin^2 \phi}, \quad \frac{a'}{1+a'} = \sigma C_l \frac{1}{4 \cos \phi} \quad (2a, b)$$

Equations (2a, b) are for a section of the blade as illustrated in Fig. 7. For a given wind speed and a constant axial induction factor  $a$  for a given station, the normal flow into the blade is constant (see Fig. 7). The swirl component  $a'$ , which is much smaller, will be essentially constant as well. Thus, Eqs. (2a, b) yield the result that the inflow angle  $\phi$ , will be constant for a given station. In this case, Eqs. (2a, b) yield

$$\sigma C_l = \text{constant.} \quad (3)$$

This result is similar to that discussed by Wilson et al. (1976); however, in that theory only the optimum case was considered. Here, the current result that  $\sigma C_l = \text{constant}$  holds for any turbine; the constant will depend, of course, on the value selected for  $a$ . The Reynolds number for any blade station is given by

$$Re = cV/\nu. \quad (4)$$

Equations (3) and (4) with the expression for the local blade solidity can be combined to yield

$$\mathcal{R} = ReC_l \quad (5)$$

where  $\mathcal{R}$  is termed here the *reduced Reynolds number*.

Equation (5) can be used to determine the Reynolds number for a station on the blade once the reduced Reynolds number  $\mathcal{R}$  is known for that station. So long as the TSR,  $V$  and  $a$  are constant,  $\mathcal{R}$  for each station will remain constant as well. The most straightforward way to determine the  $\mathcal{R}$  distribution along the blade is to set the TSR,  $V$ ,  $a$  distribution and  $C_l$  distribution. Once the blade is designed and the chord distribution is known, the  $\mathcal{R}$  distribution can be determined. Subsequent changes in the  $C_l$  distribution will not affect the  $\mathcal{R}$  distribution. Thus, for any new  $C_l$  distribution, the corresponding  $Re$  distribution can

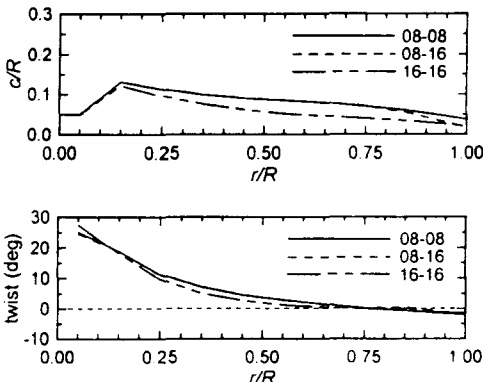


**Fig. 4 Blade chord and twist distributions for cases 08-08, 08-16, and 16-16 designed for clean conditions**

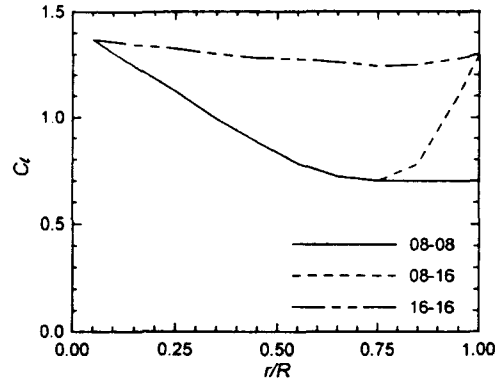


**Fig. 5 Lift coefficient distributions for cases 08-08, 08-16, and 16-16 designed for clean conditions**

be determined from the reduced Reynolds number  $\mathcal{R}$  distribution according to Eq. (5).

With this understanding of the inverse relationship between  $Re$  and  $C_l$ , it can be shown why a relatively low  $C_l$  is favored as compared with the  $C_l$  corresponding to that for best  $C_l/C_d$  for a given airfoil and Reynolds number  $Re$ . For case 16-16, the optimum  $C_l$  distribution is shown in Fig. 8(a) together with four other distributions generated by adding 0.25 and 0.125 (cases 16-16A and 16-16B) and subtracting 0.125 and 0.25 (cases 16-16C and 16-16D) from the optimum along the entire blade span. The corresponding  $C_l/C_d$  distributions are shown in Fig. 8(b). (It must be remembered that the  $C_l/C_d$  distributions shown are for  $Re$ 's that change according to Eq. (5); that is,  $Re$  is not constant but varies inversely with  $C_l$ .) The results show that case 16-16 has nearly the highest outboard  $C_l/C_d$  distribution. Cases A and B have slightly higher outboard  $C_l/C_d$  distributions, but the annual energy productions respectively changed by only  $-0.04$  percent and  $0.04$  percent relative to the baseline 16-16 case. The slightly smaller energy production of case A is due to its lower inboard  $C_l/C_d$  distribution (not shown). Cases C and D with lower  $C_l/C_d$  distributions have lower annual energy productions,  $-0.14$  percent and  $-0.43$  percent, respectively.

As Fig. 8(a) shows, the optimum  $C_l$  is near 1.3 to 1.5 at the tip station for case 16-16. This optimum  $C_l$  can be confirmed from the airfoil drag polar. At the tip, the reduced Reynolds number  $\mathcal{R}$  is  $2.4 \times 10^6$ —a constant, which could be determined from the results of any one of the corresponding  $C_l$  distributions shown in Fig. 8(a). The airfoil  $C_l - C_d$  curve for  $\mathcal{R} = 2.4 \times 10^6$  is shown in Fig. 9 along with the  $C_l - C_d$  curves for  $Re = 1 \times 10^6$ ,  $2 \times 10^6$ , and  $4 \times 10^6$ . As seen, although the best  $C_l/C_d$  for a given  $Re$  occurs at a relatively high  $C_l$ , the best  $C_l/C_d$  for  $\mathcal{R} = 2.4 \times 10^6$  occurs at a substantially lower  $C_l$  as indicated by the tangent line showing the best  $C_l/C_d$  for  $\mathcal{R} = 2.4 \times 10^6$ . Thus, it is now clear why a relatively low  $C_l$  distribution is favored. It should be added that the rate at which the blade section should be blended to a lower lift airfoil in the vicinity of the tip cannot be adequately determined with the Prandtl tip-loss model, which was used in this study. This simple model merely approximates the complex flow in the tip region. Thus, no attempt was made to refine the blade design over the last 2 percent–5 percent of span.

Another interesting result from Fig. 9 is that for constant  $\mathcal{R}$  there is a broad  $C_l$  range over which the  $C_l/C_d$  is near the maximum, thus making the PROPGA optimization method susceptible to the small noise in the airfoil performance prediction curves. Consequently, as previously described in Section 3, the resulting optimum  $C_l$  distributions from PROPGA were sometimes smoothed to provide consistent trends for comparison. As a result of this process, the optimum  $C_l$  distribution used to generate the blade using PROPID sometimes did not yield the

**Table 2** Gross annual energy production relative to the baseline 08-08 case (2473 MWh) when designed for clean conditions

		Tip Airfoil (100%)				
		100-08	100-10	100-12	100-14	100-16
Primary Airfoil (75%)	75-08	-	0.17%	0.29%	0.29%	0.30%
	75-10	-	0.46%	0.55%	0.61%	0.61%
	75-12	-	0.72%	0.75%	0.76%	
	75-14	-	0.87%	0.88%		
	75-16	-			0.97%	

absolute optimum. As Fig. 8(b) reveals, case 16-16 was indeed not optimum; however, the difference between that and the optimum was 0.04 percent in energy capture. In addition, the broad  $C_i$  range that yields best  $C_i/C_t$  for a given  $R$  provides practical design flexibility with respect to local blade solidity and roughness-effect considerations. For example, to minimize the blade solidity, the  $C_i$  distribution of a particular blade could be set near the upper  $C_i$  range, or vice versa if minimizing roughness effects were a more important design driver.

To this point, the discussion has not addressed blade surface roughness effects, which are important owing to the environment in which wind turbines operate. Wind turbine blades can be exposed to various contaminants, such as insect debris and ice accumulation at the leading edge as well as blade erosion, all of which reduce the aerodynamic performance of the airfoils used and, thereby, decrease the energy production of the rotor. To provide an indication of the reduction in energy capture due to leading-edge roughness, the blade shapes designed for clean conditions were analyzed with the airfoil data for dirty-blade conditions. PROPID predicted losses in gross annual energy production of 3.6 percent, 3.7 percent, and 4.0 percent for cases 08-08, 08-16, and 16-16, respectively. One way to reduce the roughness sensitivity of these blade shapes would be to consider roughness effects in the optimization process. In this respect, the next section will consider the merit of optimizing blade shapes not only for clean conditions but also for dirty-blade conditions.

**Blade Designs With Roughness Considerations.** Over its lifetime, a wind turbine will sometimes operate under dirty-blade ("rough") conditions. Some of the previously mentioned contaminants are seasonal and climate dependent, and their effects are usually not permanent if they are removed from the blade surface. For example, washing the blades after bug accumulation will probably restore the performance to a level closer to that of the original. With time, however, the blades will endure permanent damage, such as blade erosion, that will deteriorate their surface finish and in turn the energy production. Consequently, the rotor will operate under rough conditions that worsen with time. Is it then worthwhile to optimize the blade shapes with consideration given to ultimate operation under rough conditions?

To investigate this issue, two additional optimizations were performed. Blade shapes were optimized for rough conditions only ("rough optimizations") as well as for clean and rough conditions ("clean/rough optimizations"), which is a more reasonable assumption given the likely surface roughness condi-

**Table 3** Reduction in blade solidity relative to the baseline 08-08 case ( $\sigma = 0.077$ ) when designed for clean conditions

		Tip Airfoil (100%)				
		100-08	100-10	100-12	100-14	100-16
Primary Airfoil (75%)	75-08	-	1.4%	2.7%	3.8%	5.0%
	75-10	-	9.2%	10.6%	12.0%	13.0%
	75-12	-	17.8%	18.8%	19.8%	
	75-14	-		23.8%	24.9%	
	75-16	-			29.2%	

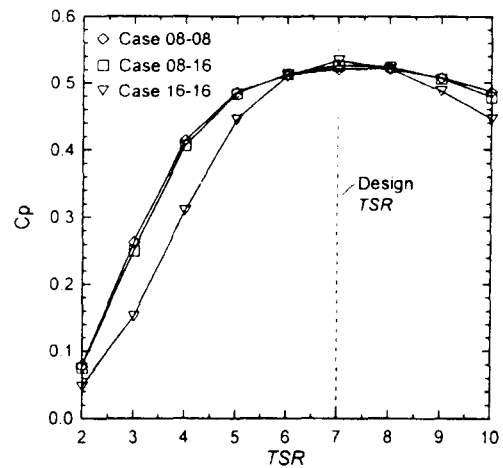


**Fig. 6** Power coefficient for a range of TSR for cases 08-08, 08-16, and 16-16 all designed for clean conditions and a TSR of 7

tion of a blade over its lifetime. In the clean/rough optimization, the figure of merit was the average energy production between clean and rough performance. The results for the gross annual energy production (GAEP) of these two additional optimizations along with the previous results for the clean conditions ("clean optimization") are presented in Fig. 10. In this figure, a clean analysis means that the optimized blade shape was analyzed with clean airfoil data and the rough analysis corresponds to the rough conditions. For reference, the axis of the gross annual energy production in Fig. 10 represents approximately an eight percent difference in energy capture.

Much can be gleaned from the trends of Fig. 10 for the four selected cases shown. As expected, including roughness effects in the optimization process provided blade shapes with a smaller spread between their clean and rough performance. For example, the baseline (case 08-08) when optimized for rough conditions suffers only a 0.8 percent decrease in performance (clean versus rough) as compared with a 3.6 percent decrease when optimized for clean conditions. Note, however, that the performance losses due to roughness are smaller than the expected 5 percent–10 percent reduction in energy capture for variable-speed rotors equipped with the traditionally used airfoils that were originally designed for aircraft applications (Tangler and Somers, 1995; Tangler, 1996). The current airfoils have lower losses because they were designed for the conditions experienced by wind turbines.

Figure 10 also indicates the benefit of considering rough performance in the optimization process. The rough-optimized blades, that is, the blades optimized for rough conditions, provided greater average energy production as compared with the clean-optimized blades. The best average performance came from the clean/rough-optimized blades for all cases, with case 12-16 being the best overall case. More specifically, the clean/rough-optimized blades provided average energy productions that were 0.44 percent, 0.68 percent, 0.50 percent, and 0.28

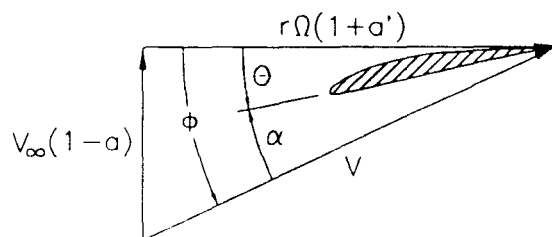


**Fig. 7** Flow diagram for a section of the blade

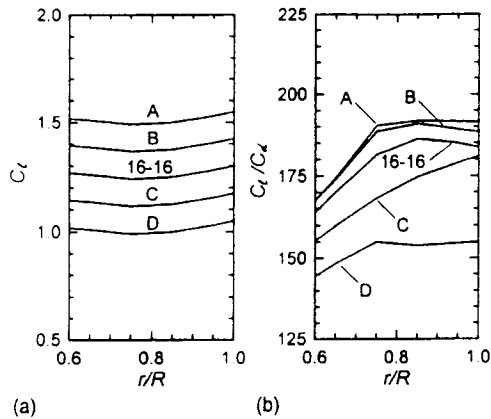


Fig. 8(a) Outboard  $C_t$  distribution for the case 16-16 (clean optimization) together with four other  $C_t$  distributions generated by adding  $\pm 0.125$  and  $\pm 0.25$  to the optimum and (b) the corresponding outboard  $C_t/C_d$  distributions

percent greater than the clean-optimized blades for cases 08-08, 08-16, 12-16, and 16-16, respectively.

Including roughness effects in the optimization process affected the blade solidity. For the cases with the low-lift 75-08 primary airfoil, the rough blades have approximately a 20 percent reduction in solidity as compared with the clean blades. When higher lift airfoils were used at the primary station in the rough optimization, the blade solidity changed negligibly for case 12-12 and increased by 7 percent and 15 percent for cases 12-16 and 16-16, respectively. These changes in blade solidity can be traced to the shift in the  $C_t$  for which the best  $C_t/C_d$  condition occurs. Figure 11 shows the drag polars for three primary airfoils for clean and rough conditions at  $Re = 2 \times 10^6$ . The tip airfoil polars follow similar trends. As expected, the  $C_t$  corresponding to the best  $C_t/C_d$  for each airfoil depends on the condition—clean or rough. More specifically, the  $C_t$  for best  $C_t/C_d$  under rough conditions is approximately 1.3 for the three airfoils shown in Fig. 11. This  $C_t$  value is either greater or smaller than the design  $C_t$  for the airfoils 75-08, 75-12, and 75-16, namely  $C_t \approx 0.8, 1.2,$  and  $1.6,$  respectively. Leading-edge roughness yielded an increase in  $C_t$  for best  $C_t/C_d$  for the 75-08 and 75-12 airfoils, albeit a small increase for airfoil 75-12. For the 75-16 airfoil, there is a decrease in  $C_t$  for best  $C_t/C_d$ . These trends in  $C_t$  for best  $C_t/C_d$  can be used to explain the changes in blade solidity for the rough and clean/rough blades as compared with the clean blades. Thus, for high-

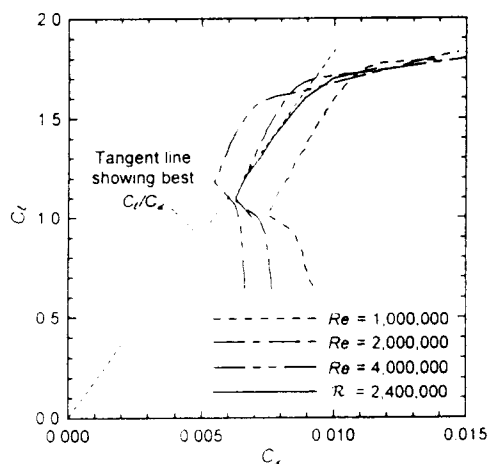


Fig. 9 Airfoil 100-16 performance characteristics for  $Re = 1 \cdot 10^6, 2 \cdot 10^6, 4 \cdot 10^6,$  and for  $R = 2.4 \cdot 10^7$

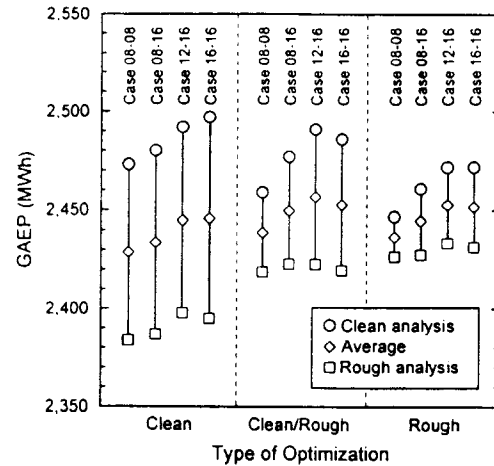


Fig. 10 Gross annual energy production (GAEP) for cases 08-08, 08-16, 12-16, and 16-16 designed with different types of optimization

lift airfoils, such as the 75-16, the rough-optimized blades have a lower  $C_t$  distribution as compared with the clean optimized blades and, consequently, yield blades with higher solidity. The opposite trend occurs for blades designed with low to moderate-lift airfoils, such as the 75-08 and 75-12. For the clean/rough-optimized blades, the increase/decrease in blade solidity was nearly half that for the rough-optimized blades. The effects on solidity were less since roughness effects did not totally dominate the blade optimization process as the blades had to perform well also under clean-blade conditions.

#### Trade-off Between Clean and Rough Performance.

Based on the previous results, which shed light on roughness effects in design, there is clearly a trade-off between energy production and blade solidity when roughness effects are considered. Rough-blade designs with high-lift airfoils provide a small performance gain at a cost of a much larger increase in blade solidity as compared with clean-optimized blades. For large and medium-size wind turbines, material costs are an important factor, and consequently a small increase in energy capture on the order of 0.3 percent might not justify a 8 percent increase in blade solidity. Accordingly, optimizing the blade shapes of large and medium size HAWTs that make use of high-lift airfoils for wind turbine applications based on clean-blade performance only seems an appropriate design approach. The use of a primary airfoil having moderate lift (e.g., 75-12

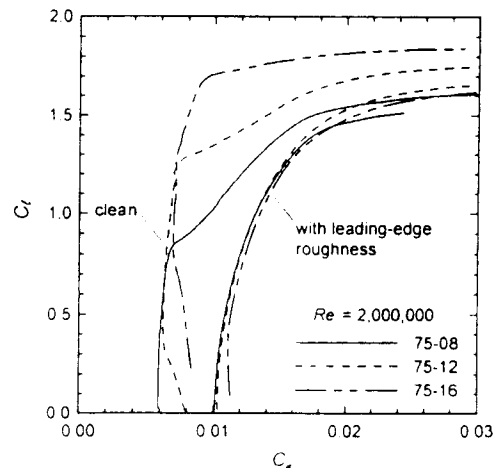


Fig. 11 Predicted drag polars for three primary airfoils under clean and rough conditions at  $Re = 2 \cdot 10^6$

airfoil) in a clean/rough optimization is perhaps a better design approach since it provides a larger increase in energy production at no increase (or even a small decrease) in blade solidity. In the case where design constraints such as structural considerations require blades of larger solidity, lower lift airfoils should then be favored. When lower lift airfoils are used in the design, however, a clean/rough optimization should be used even though it will produce blades of lower solidity than a clean optimization.

The merit of including roughness considerations in the optimization of blades that make use of low to moderate-lift airfoils is not obvious a priori since as indicated in Fig. 11 high-lift airfoils are more affected by leading-edge roughness effects. Figure 11 also suggests that a blade design based on high-lift airfoils will favor a lower  $C_l$  in a clean/rough optimization as indicated by the decrease in  $C_l$  for best  $C_l/C_d$  under rough conditions. Therefore, it is important to consider the lift range for best  $C_l/C_d$  for both clean and rough conditions in determining the roughness sensitivity of an optimized blade shape. In this respect, moderate and especially low-lift airfoils achieve their best  $C_l/C_d$  at higher  $C_l$  when rough than clean, and consequently clean/rough optimization is more suited for blades designed with such airfoils. This last observation is confirmed by the results for the average performance shown in Fig. 10. Indeed, Fig. 10 indicates that the differences in average energy production for cases 08-08 and 08-16 between the different types of optimization is larger than for cases 12-16 and 16-16.

## 5 Conclusions

The results of this work show that for a series of airfoils that covered a range in  $C_l$  and  $C_l/C_d$  the differences in annual energy for a large variable-speed wind turbine were slight, on the order of one percent at most, but these differences were significant relative to a 2.5 percent–3.5 percent gain obtained by setting the airfoil profile drag to zero. It is important to emphasize that the airfoils designed for this study were specifically tailored for wind turbine applications. Therefore, the differences in energy production would have been greater if less suitable airfoils (those originally designed for aircraft applications) were considered as well. The blade solidity, however, was greatly affected by the airfoil series. High-lift airfoils with their best  $C_l/C_d$  occurring at high  $C_l$  produced blades with low solidity since high  $C_l$  is favored, and vice versa. It was shown that blade element/momentum theory can be used to yield a relationship between the local blade solidity and the operating  $C_l$ . This equation when combined with that for the Reynolds number gives an equation for what has been called here the reduced Reynolds number  $\mathcal{R}$ . When the airfoil data is plotted for constant  $\mathcal{R}$ , it is found that the best performance is obtained when the blade is designed to operate near the best  $C_l/C_d$  for a given  $\mathcal{R}$  that depends on the wind speed, blade TSR and axial inflow for a given blade section.

Roughness effects were found to be relatively small with losses on the order of three to four percent for the blade shapes optimized based on their clean-blade performance. This result was found to be lower than the projected loss in energy capture for variable-speed operation documented in the literature, thus indicating that the airfoil design process used in this study was successful in its attempt to minimize roughness effects. It was also found that optimizing blade shapes based on clean and rough performance (clean/rough optimizations) was primarily useful for designs based on primary airfoils having a low to moderate lift range. An optimization process that is based only on the clean conditions is sufficient for blades designed with high-lift airfoils at both the primary and tip stations. Such a design yielded the best overall energy capture under clean conditions but suffered the most from roughness effects. A better compromise, which provided a 0.5 percent increase in average annual energy production, was found to be a blade that is opti-

mized for best average performance between clean and rough conditions with a moderate-lift primary airfoil and a high-lift tip airfoil. As previously mentioned, however, blending to a lower lift airfoil at the tip of the blade should be favored in order to reduce profile drag losses. Unless some design constraints require large blade solidity, low-lift airfoils should not be used in the blade design for a variable-speed wind turbine if energy production is to be maximized.

As expected and as this study has indicated, high  $C_l/C_d$  is a desirable airfoil characteristic for variable-speed wind turbines. To achieve high  $C_l/C_d$  values while considering roughness effects, a moderate amount of laminar flow, e.g., 30 percent chord, on the airfoil upper surface at low  $C_l$  and a relatively small thickness are additional desirable airfoil characteristics. Given the rather small effect of leading-edge roughness on the performance of variable-speed HAWTs, airfoils with larger amounts of laminar flow on the upper surface could perhaps prove to be quite acceptable. Furthermore, it is quite clear from the results of this study that high-lift airfoils were successful in maximizing energy capture, especially when used toward the tip. At the primary station, however, an airfoil with a moderate lift range provides a better compromise between clean and rough performance.

Although this study has focused on a large variable-speed HAWT, the general conclusions presented here should apply to other size wind turbines, especially larger wind turbines (on the order of 1 MW). For smaller variable-speed HAWTs, it is suggested that a similar airfoil/blade-shape optimization procedure as outlined be performed. Small wind turbines operate at low Reynolds numbers, and consequently roughness effects are likely to be more important and may change some of the conclusions presented here. In particular, for low Reynolds number applications, thinner airfoils with less laminar flow on the upper surface could be favored.

## Acknowledgments

The support of the National Renewable Energy Laboratory under Subcontract XAF-4-14076-03 is gratefully acknowledged. Also, the several discussions with James L. Tangler of NREL proved to be quite helpful during the course of this work.

## References

- Björk, A., 1988, "Airfoil Design for Horizontal Axis Wind Turbines," *Proceedings of the Second IEA Symposium on Joint Action on Aerodynamics of Wind Turbines*, Lyngby, Denmark, pp. 204–230.
- Björk, A., 1989, "Airfoil Design for Variable RPM Horizontal Axis Wind Turbines," *Proceedings of the 1989 European Wind Energy Conference (EWEC)*, Glasgow, Scotland.
- Drela, M., 1989, "XFoil: An Analysis and Design System for Low Reynolds Number Airfoils," *Lecture Notes in Engineering: Low Reynolds Number Aerodynamics*, T. J. Mueller, ed., Vol. 54, Springer-Verlag, New York.
- Drela, M., 1990, "Elements of Airfoil Design Methodology," *Progress in Astronautics and Aeronautics: Applied Computational Aerodynamics*, P. A. Henne, ed., Vol. 125, AIAA, Washington, DC, pp. 167–189.
- Hibbs, B., and Radkey, R. L., 1983, "Calculating Rotor Performance with the Revised PROP Computer Code," *Horizontal-Axis Wind System Rotor Performance Model Comparison—A Compendium*, Wind Energy Research Center, Rockwell International, Rocky Flats Plant, Golden, CO, RFP-3508, UC-60.
- Hill, G. C., and Garrard, A. D., 1989, "Design of Aerofoils for Wind Turbine Use," *Proceedings of the 1989 European Wind Energy Conference (EWEC)*, Glasgow, Scotland.
- Jameson, P., and Rawlinson-Smith, R., 1994, "High Lift Aerofoils for Horizontal Axis Wind Turbines," *British Wind Energy Association (BWEA) 16 Conference*, Stirling, England.
- Madsen, H. A., and Rasmussen, F., 1992, "Experiences in Airfoil Analysis and Design," *Proceedings of the Sixth IEA Symposium on the Aerodynamics of Wind Turbines*, Petten, Netherlands.
- Selig, M. S., and Maughmer, M. D., 1992, "Generalized Multipoint Inverse Airfoil Design," *AIAA J.*, Vol. 30, No. 11, pp. 2618–2625.
- Selig, M. S., and Tangler, J. L., 1995, "Development and Application of a Multipoint Inverse Design Method for Horizontal Axis Wind Turbines," *Wind Engineering*, Vol. 19, No. 2, pp. 91–105.

Selig, M. S., Maughmer, M. D., and Somers, D. M., 1995, "A Natural-Laminar-Flow Airfoil for General-Aviation Applications," *Journal of Aircraft*, Vol. 32, No. 4, pp. 710-715.

Selig, M. S., and Coverstone-Carroll, V. L., 1996, "Applications of a Genetic Algorithm to Wind Turbine Design," *ASME Journal of Energy Resources Technology*, Vol. 118, pp. 22-28.

Somers, D. M., 1986, "Design and Experimental Results for the S805 Airfoil," Airfoils, Inc., State College, PA.

Somers, D. M., 1987, "Design and Experimental Results for the S809 Airfoil," Airfoils, Inc., State College, PA.

Somers, D. M., 1992, "Subsonic Natural-Laminar-Flow Airfoils," *Natural Laminar Flow and Laminar Flow Control*, R. W. Barnwell and M. Y. Hussaini, eds., Springer-Verlag, New York, pp. 143-175.

Somers, D. M., 1994, "Design and Experimental Results for the S814 Airfoil," Airfoils, Inc., State College, PA.

Tangler, J. L., and Somers, D. M., 1995, "NREL Airfoil Families for HAWTs," *American Wind Energy Association Windpower '95 Conference*, Washington, DC.

Tangler, J. L., 1996, "Influence of Pitch, Twist, and Taper on a Blade's Performance Loss Due to Roughness," *American Wind Energy Association Windpower '96 Conference*, Denver, CO.

Timmer, W. A., and van Rooy, R. P. J. O. M., 1992, "Thick Airfoils for HAWTs," *J. of Wind Engineering and Industrial Aerodynamics*, Vol. 39, pp. 151-160.

Wilson, R. E., Lissaman, P. B. S., and Walker, S. N., 1976, "Aerodynamic Performance of Wind Turbines," Department of Mechanical Engineering, Oregon State University, Corvallis, OR, National Science Foundation, Research Applied to National Needs (RANN), Rep. No. NSF/RA-760228, NTIS PB 238594.

Wilson, R. E., 1994, "Aerodynamic Behavior of Wind Turbines," *Wind Turbine Technology*, D. A. Spera, ed., Chapter 5, ASME Press, New York, pp. 215-282.



The American Society of  
Mechanical Engineers

# ASME COUPON BOOKS

Use coupons to purchase all ASME publications — including special publications, codes and standards, and technical papers (preprints). Use coupons to save money. Technical papers cost less when you purchase them with coupons! One coupon may be redeemed for one technical paper. That's a savings of \$.50 for members, \$1.00 for non-members (off the regular price for preprints).

TECHNICAL PAPERS (PREPRINTS) COUPON BOOK  
CONTAINS 10 COUPONS ORDER No. CB0001  
\$40 (ASME MEMBERS) / \$80 (NON-MEMBERS)

PUBLICATIONS COUPON BOOK  
CONTAINS 10 COUPONS (\$10 EACH)  
ORDER No. CB0002  
\$100 (MEMBER & NON-MEMBER)

TELEPHONE  
800-THE-ASME  
(800-843-2763)  
USA & CANADA  
95 800-843-2763  
MEXICO  
201-882-1167  
OUTSIDE No. AMERICA

FAX  
201-882-1717 OR  
201-882-5155

E-MAIL  
infocentral@asme.org

MAIL  
ASME  
22 LAW DRIVE  
P.O. Box 2300  
FAIRFIELD, NEW JERSEY  
07007-2300